This is the accepted version of the article:

Pedersen, J.G.; Cummings, A.W.; Roche, S.. Anisotropic behavior of quantum transport in graphene superlattices: Coexistence of ballistic conduction with Anderson insulating regime. Physical Review B - Condensed Matter and Materials Physics, (2014). . : - . 10.1103/PhysRevB.89.165401.

Available at: https://dx.doi.org/10.1103/PhysRevB.89.165401

Anisotropic Behavior of Quantum Transport in Graphene Superlattices: Coexistence of Ballistic Conduction with Anderson Insulating Regime

Jesper Goor Pedersen[1,2] Aron W. Cummings[2], and Stephan Roche[2,3]
[1] *DTU Nanotech – Department of Micro- and Nanotechnology,*
Technical University of Denmark, DK-2800 Kgs. Lyngby, Denmark
[2] *Institut Català de Nanociència i Nanotecnologia (ICN2),*
Campus de la UAB, Edifici ICN2, 08193 Bellaterra, Barcelona, Spain
[3] *ICREA - Institucio Catalana de Recerca i Estudis Avancats, 08010 Barcelona, Spain*

(Dated: January 28, 2014)

We report on the possibility to generate highly anisotropic quantum conductivity in disordered graphene-based superlattices. Our quantum simulations, based on an efficient real-space implementation of the Kubo-Greenwood formula, show that in disordered graphene superlattices the strength of multiple scattering phenomena can strongly depend on the transport measurement geometry. This eventually yields the coexistence of a ballistic waveguide and a highly resistive channel (Anderson insulator) in the same two-dimensional platform, evidenced by a σ_{yy}/σ_{xx} ratio varying over several orders of magnitude, and suggesting the possibility of building graphene electronic circuits based on the unique properties of chiral massless Dirac fermions in graphene.

PACS numbers: 73.23.-b, 72.15.Rn, 73.21.Cd

In recent years, graphene has received a great deal of interest for its unusual electrical transport properties, including phenomena such as Klein tunneling [1] and weak antilocalization [2]. These phenomena preclude the formation of an insulating state at low levels of disorder, in contrast to traditional 2D metallic systems, which are predicted to exhibit an insulating state for arbitrarily small disorder strengths [3, 4]. This unique behavior makes graphene a promising material for a wide range of next-generation technological applications [5]. One challenging research objective is to maximize the transport anisotropy of graphene, such that it remains a good conductor along one direction while being much more resistive along the other. Such control over the transport properties could be used to direct charge flow and thus build electronic circuits or waveguides [6], optical circuits [7], or communications devices [8]. For most types of scattering sources, the transport properties in disordered graphene remain isotropic. Meanwhile, more complex forms of disorder, such as structural deformations produced by interaction with a substrate [9, 10] or chemical doping [11], can produce only a moderate transport anisotropy in graphene.

A way around this problem involves the creation of graphene superlattices, which are formed from a periodic modulation of the electrical, mechanical, or chemical properties of pristine graphene. Indeed, it has been theoretically predicted that a strong anisotropy in the Fermi velocity of graphene can be induced by suitably patterned periodic modifications of the graphene surface [12]. Based on this work, the construction of novel types of graphene electronic devices and circuits from structurally-perfect engineered superlattices was foreseen, attracting a lot of attention [13]. To date however, the inherent and uncontrollable disorder introduced through conventional lithography techniques and top-down patterning approaches has impeded the realization of these graphene-based superlattices, whose novel transport and device characteristics depend entirely on bandstructure engineering [14–16], and thus are highly sensitive to disorder. In particular, features relying on the emergence of a band gap [17] have remained elusive.

In this Letter, we wish to advocate a different approach to nanostructuring graphene, where instead of considering disorder an inevitable drawback, it may in fact serve as beneficial for tuning the properties of graphene. While structural disorder inherent to any fabricated graphene-based superlattice (such as antidot lattices and nanomeshes) jeopardizes the control of bandstructure features, we demonstrate that at the same time disorder enables the coexistence of transport regimes which are generally incompatible in conventional conducting materials. By using efficient numerical methodologies, the scaling properties of quantum transport through disordered graphene-based superlattices are computed and are shown to become exceedingly anisotropic, resulting in the coexistence of a ballistic transport channel in one direction and a highly resistive channel in the other. These results suggest that disorder, rather than being an inevitable problem, could instead serve as a new inherent tool in the experimental realization of nanostructured graphene, giving rise to unique transport properties of chiral massless Dirac fermions. We note that similar ideas have been proposed within the field of photonic crystals [18].

We consider a disordered, rectangular lattice of perforations in an otherwise pristine graphene sheet. A given superlattice is referred to via parameters $\{N_x, N_y\}$, with N_μ denoting the average number of hexagons between the center of the holes along each direction. The lattice con-

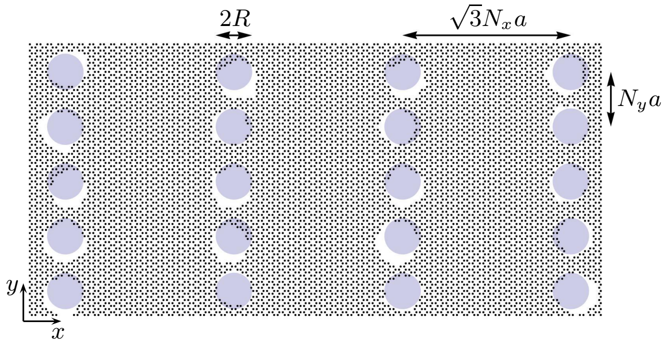

FIG. 1: Geometry of a representative domain of a disordered $\{16, 9\}$ superlattice. Carbon atoms are indicated with black points. The blue shading indicates the position of holes in the pristine geometry.

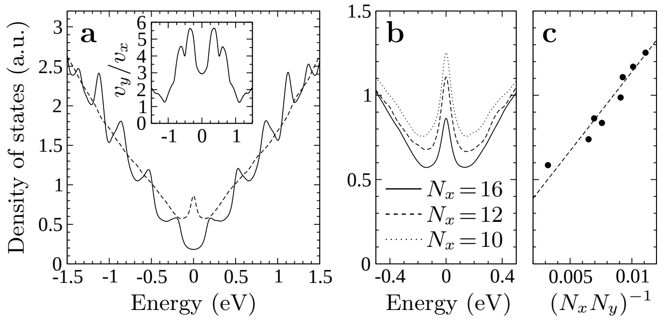

FIG. 2: (a) Density of states of a pristine (solid line) and a disordered (dashed line) $\{16, 9\}$ superlattice. Note the absence of any signatures of van Hove singularities for the disordered structure. The inset shows the ratio of group velocities v_y/v_x of the pristine superlattice. (b) Density of states near the Dirac point for three different disordered superlattices $\{N_x, 9\}$. (c) Density of states at the Dirac point for several disordered superlattices, illustrating the approximately linear dependence of the Dirac point DOS on the hole density.

stants of the pristine superlattice are thus $A_x = \sqrt{3}N_x a$ and $A_y = N_y a$, respectively, with $a = 0.246$ nm the graphene lattice constant. The average size of the antidots is defined via the radius R, which we set to $R = 3a$ for all results presented. We consider superlattices for which $N_x/N_y > 1$ and refer to the y and x directions as the *easy* and the *hard* directions, respectively. Disorder is included via the parameters δ_x, δ_y, δ_R, p_{rem}, and N_{rem}. Here, δ_x, δ_y and δ_R denote the widths of random fluctuations in the centres and radii of holes, respectively. Edge disorder along the holes is added via an iterative process repeated N_{rem} times, in which edge atoms (defined as any atom with less than three nearest neighbours) are removed with probability p_{rem}. We remove any dangling bonds in the geometry, i.e., all carbon atoms have at least two nearest neighbours. While structural relaxation is not included in the simulations, the absence of dangling bonds leads us to expect only a minor influence of potential geometrical relaxation [19]. Throughout this Letter we take $\delta_x = \delta_y = 2a$, $\delta_R = 0.5a$, $p_{\mathrm{rem}} = 5\%$, and $N_{\mathrm{rem}} = 2$. An example of a disordered $\{16, 9\}$ superlattice is illustrated in Fig. 1. Note that the figure only shows a small, representative domain of the full structure used in the calculations, which contains several millions of atoms. We stress that while we only show results for $N_x > N_y$, we have confirmed that the results do not depend qualitatively on the orientation of the superlattice with respect to the graphene sheet.

To model the properties of the proposed structures, we employ a nearest-neighbour tight-binding model with the hopping element $t = -3$ eV and set the on-site energy to zero. Transport properties are determined numerically via an efficient, order-N real-space Kubo approach [20–23]. The time- and energy-dependent diffusion coefficient is calculated via $D_x(E, t) = \Delta X(E, t)^2/t$, with the mean quadratic displacement given as $\Delta X(E, t)^2 = \mathrm{Tr}[\delta(E - \hat{H})|\hat{X}(t) - \hat{X}(0)|^2]/\rho(E)$, where $\rho(E) = \mathrm{Tr}[\delta(E - \hat{H})]$ represents the total density of states. Traces are approximated via initial random phase states and the Lanczos method [24], while the time evolution operator is expanded in Chebyshev polynomials. We use 1500 iterations in the Lanczos method, with broadening included via an imaginary part $\eta = 0.04$ eV of the energy, while the number of Chebyshev polynomials is determined by requiring unitarity of the time evolution operator (within an error of $< 10^{-6}$). The Kubo conductivity, including quantum interference effects, can be calculated from the diffusion coefficients as $\sigma_{xx}(E, t) = e^2\rho(E)D_x(e, t)/2$, while the semi-classical conductivity reads $\sigma_{xx}^{\mathrm{SC}}(E, t) = e^2\rho(E)\max_t D_x(E, t)/2$. Transport properties along the y-direction are calculated similarly.

In Fig. 2a, solid lines illustrate the density of states (DOS) for a pristine $\{16, 9\}$ superlattice. Note the quasi-one-dimensional nature of the DOS with clear signatures of van Hove singularities. This is consistent with a picture of the superlattice as an array of weakly coupled nanoribbons aligned along the easy direction. The large aspect ratio of the superlattice unit cell results in a substantial anisotropy of the group velocity v_y/v_x, as illustrated in Fig. 2a(inset). Note that for larger energies (not shown), such anisotropy is much less pronounced, as expected from the suppression of band structure effects for energies where the electron wavelength becomes much smaller than the hole spacing. While an anisotropic Fermi velocity should affect transport properties, any effect relying critically on periodicity is bound to be quenched significantly in experimental realizations due to the presence of disorder.

We here consider this issue by focusing on lattices displaying significant structural imperfections, inspired by recent experimental fabrication and characterization of graphene nanomeshes (or antidot lattices) [25]. In stark

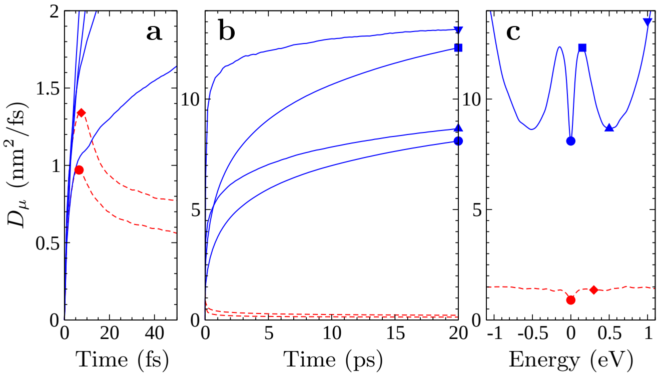

FIG. 3: Time- and energy-dependent diffusion coefficients D_μ for a disordered $\{16,9\}$ superlattice. Solid blue (red dashed) lines show the diffusion coefficient along the easy (hard) direction. (a) Short-time behaviour of D_μ, illustrating strong localization along the hard direction. (b) Long-time behaviour of D_μ, illustrating quasi-ballistic transport along the easy direction. (c) Maximum diffusion coefficients within the simulation time span, shown versus energy. The symbols indicate the energies to which results in panels a and b correspond.

contrast to the pristine case, the DOS of such disordered structures (dashed line in Fig. 2a) becomes largely featureless, except for the presence of a peak at the Dirac point. The disorder is thus sufficiently strong to wash out the characteristics of the bandstructure associated with the superlattice. In Fig. 2b we show a closer view of the zero-energy DOS peak, for three different values of N_x. While the DOS resembles that of bulk graphene with short-range impurities [26], the source of the zero-energy peak is slightly different in our case, as we explicitly avoid dangling bonds in our geometries. Instead, we attribute the zero-energy peak to states emerging due to local sublattice imbalances around the holes. These midgap states are localized predominantly on the hole edges [19, 27]. Consistent with this picture, we illustrate in Fig. 2c the proportionality of the zero-energy DOS with the density of holes, quantified here via the dimensionless quantity $1/(N_xN_y)$.

As discussed above, the disorder considered is strong enough to quench any effects emerging due to the periodicity of the superlattice (such as anisotropic group velocities). Instead, the scattering sources are determined by the randomness in the position, radius, and internal geometries of the holes. Despite the largely featureless density of states, this results in drastically different transport properties along the two directions, as illustrated in Fig. 3. Here, we show the diffusion coefficients $D_\mu(E,t)$ for a disordered $\{16,9\}$ superlattice, for different energies within 1 eV of the Dirac point. Along the easy direction, the time dependence of the diffusion coefficients exhibits (within our accessible timescale of 20 ps) a quasiballistic behavior since D_μ does not saturate (see Fig. 3a and b, blue solid curves). In sharp contrast, along the hard axis $D_\mu(E,t)$ manifests a weak increase at short times (up to the range of 20 fs) before reaching its maximum value (from which one evaluates the elastic mean free path) and then strongly decays in time, as a result of quantum interferences and localization pheneomena (Fig. 3a and b, red dashed curves) [32].

We note that the total elapsed time of 20 ps considered in our calculations corresponds to sample dimensions on the order of 800 − 1000 nm along the easy direction and 100 − 180 nm along the hard direction (using $L_\mu(E)=2\sqrt{t_{\max}D_\mu(E,t_{\max})}$). These results suggest that not only will conductivities along the two directions be of different orders of magnitude, but the temperature dependence should also indicate different transport regimes. In particular, for longer elapsed times (corresponding to wavepacket exploration of larger samples), a metallic behaviour for $\sigma_{yy}(T)$ should be measured along one direction, while an insulating behavior for $\sigma_{xx}(T)$ should develop along the other.

In Fig. 3c we show the maximum value of the diffusion coefficient within the simulated time span. We attribute the sharp dip near zero energy to the localized zero-energy modes discussed above in relation to the DOS. As these states are predominantly localized around the hole edges, they will naturally be more sensitive to multiple scattering phenomena. Indeed, we find that the peak in the mean free path coincides perfectly with the minimum of the DOS on either side of the Dirac point (see Fig. 4). Additionally, we find that increasing the edge disorder further deepens the zero-energy feature, while features outside the energy range of the DOS peak are comparably much less affected.

We extend our analysis by superimposing a random distribution of long range impurities over the disordered superlattice potential. This enforces a saturation of the diffusion coefficients along both directions, giving access to effective mean free paths in the x and y-directions. We consider the addition of N_{I} long-range impurities, the effect of which is included in the on-site energies $V_n=\langle n|H|n\rangle$ as $V_n=\sum_i^{N_{\mathrm{I}}}\epsilon_i\exp(-|\mathbf{r}_n-\mathbf{r}_i|^2/(2\xi^2))$, where ξ sets the effective range, while the $\epsilon_i\in[-W/2,W/2]$ are randomly distributed [28–30]. We take usual parameters $W=|t|$ and $\xi=\sqrt{3}a$, and consider a very low impurity concentration of 0.02%, sufficient to give rise to a diffusive regime but low enough so that scattering remains dominated by the superlattice-driven random potential. The elastic mean free path is calculated from the maximum of the diffusion coefficient, $l_e(E)=D_{\max}(E)/(2v_F)$, with v_F the Fermi velocity and $D_{\max}(E)$ the maximum of the average diffusion coefficient, $D(E,t)=(D_x(E,t)+D_y(E,t))/2$. To study the transport anisotropy of the designed structures, we define the directional effective mean free paths $l^*_\mu(E)\equiv\max_t D_\mu(E,t)/(2v_\mu(E))$. We note that while we find a significant renormalization of the Fermi velocity for pristine superlattices, such an effect, as discussed above, is

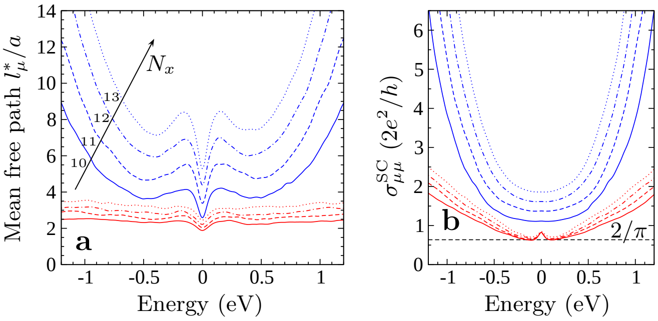

FIG. 4: (a) Directional mean free paths $l^*_{e,\mu}$, in units of the graphene lattice constant, for disordered superlattices $\{N_x, 9\}$ with long-range impurities. Red lines show results for the 'hard' direction, $l^*_{e,x}$, while blue lines indicate results for the 'easy' direction, $l^*_{e,y}$. (b) Corresponding semiclassical conductivities, in units of $2e^2/h$, along each direction.

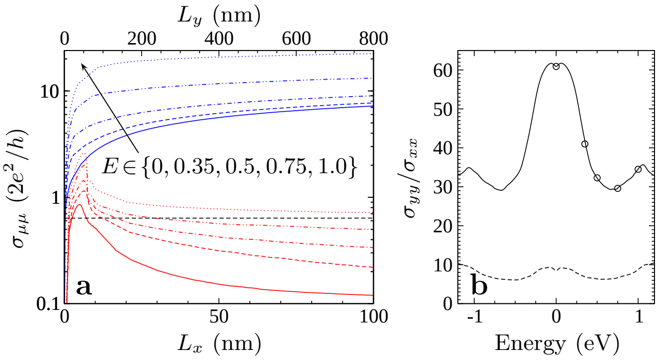

FIG. 5: (a) Conductivity vs length for the disordered $\{16, 9\}$ superlattice. Red lines show results for the 'hard' direction, σ_{xx}, while blue lines indicate results for the 'easy' direction, σ_{yy}. Note the logarithmic scale on the ordinate. The horizontal dashed line indicates the minimum value $\sigma^{\rm SC}_{\rm min}$ in the absence of quantum interference. (b) Ratio of conductivities calculated at the maximum lengths of the simulated time span of 20 ps. The dashed line indicates the ratio when quantum interference effects are neglected for $\sigma_{\rm xx}$. Circles indicate the energies corresponding to the results in panel a.

absent for the level of disorder we consider here. We thus use the pristine graphene Fermi velocity in all calculations of mean free paths.

As evident in Fig. 4a, the anisotropy of the structure is readily apparent in the mean free paths l^*_μ, which not only differ in magnitude, but also exhibit distinct energy dependencies, with $l^*_x(E)$ almost featureless except for the presence of a small dip near zero energy. The energy dependence of l^*_y is considerably richer, with a behaviour similar to that seen in Fig. 3c, albeit with the peak and subsequent dip slightly smeared by the addition of long-range impurities. Our interpretation of the energy dependence of l^*_y remains the same as that discussed above in relation to Fig. 3c. The directional mean free paths in Fig. 4a are shown for increasing values of N_x, illustrating how this parameter serves as an effective way of tuning the anisotropy of the scattering-mediated transport. Indeed, l^*_y is approximately linearly dependent on N_x for energies near the Dirac point. We stress that even though the directional mean free paths are of similar magnitude near the Dirac point, the transport regimes remain distinctly different, namely diffusive along the easy direction while strongly localized along the hard direction. The corresponding semi-classical conductivities are shown in Fig. 4b, illustrating how, along the easy direction, the distinct behaviour of the mean-free path near zero energy is counteracted by the corresponding density of states, resulting in a largely flat plateau near the Dirac point. Note that the width of the plateau decreases as N_x is increased, while the height of the plateau increases approximately linearly with N_x. The semi-classical conductivity along the hard direction shows an entirely different energy dependence, with a slight peak near the Dirac point. We find that the zero-energy semi-classical conductivity is nearly independent of N_x, and shows an approximately quadratic dependence on N_x at non-zero energies near the Dirac point. The horizontal dashed line in Fig. 4b indicates the minimum value, $\sigma^{\rm SC}_{\rm min} = 4e^2/\pi h$, a value that has been demonstrated to fix the minimum semi-classical conductivity in disordered graphene [31, 32].

While the ratios $\sigma^{\rm SC}_{yy}/\sigma^{\rm SC}_{xx}$ of the semi-classical conductivities shown in Fig. 4 are less than an order of magnitude, transport along the hard direction enters the Anderson localized regime, which will further maximize the resulting transport anisotropy. To illustrate this behavior, we study the disordered $\{16, 9\}$ superlattice in absence of long-range impurities. Fig. 5a shows the conductivities $\sigma_{\mu\mu}$ as a function of the sample dimensions L_x and L_y. The location of the minimum semi-classical conductivity $\sigma^{\rm SC}_{\rm min} = 4e^2/\pi h$, indicated by the horizontal dashed line in Fig. 5a, separates the different transport regimes. For $\sigma_{\mu\mu} > \sigma^{\rm SC}_{\rm min}$ the system remains metallic and the conductivity remains finite down to zero temperature, whereas the length-dependent decay of $\sigma_{\mu\mu}$ below $\sigma^{\rm SC}_{\rm min}$ is evidence of the dominant role played by quantum interferences, which successively drive the electronic state from weak localization to the strong (Anderson) localization regime.

Note that outside the initial transition regime, conductivity along the easy direction becomes more than an order of magnitude larger than along the hard direction within our accessible computational time (or length) scales. This trend is illustrated in Fig. 5b, where the ratio $\sigma_{yy}(L_{y,\rm max})/\sigma_{xx}(L_{x,\rm max})$ is shown. The strongest anisotropy is seen near the Dirac point, where scattering due to edge states around the holes is most pronounced. As we further upscale sample size, the transport anisotropy $\sigma_{yy}(L_y)/\sigma_{xx}(L_x)$ will continuously increase. A crossover to very strong anisotropy will take place once the sample size along the hard direction reaches the directional localization length ξ_x. This length scale can be estimated using $\xi_x(E) = l^*_x(E)\exp(\pi h\sigma^{\rm SC}_{xx}(E)/(2e^2))$ [3]. For the $\{16, 9\}$ superlattice in absence of long-range impurities, we find that the localization length along the hard direction is of the order of 10 nm. In an experiment, our results suggest that depending on the measurement geometry, the low temperature conductivity could manifest a variable range hopping in the hard direction (similar to the case of damaged graphene [33]), whereas a metallic behaviour (and finite conductivity value) will be measured in the perpendicular direction. To date such strong conductivity anisotropy has never been reported in metallic materials, or disordered graphene. By applying an external magnetic field, one may further tailor the anisotropy in the semiclassical regime [34], while the modulation of magnetotransport features at low fields and the quantum Hall effect at high fields both deserve further consideration. In conclusion, we have shown that disorder, while destroying anisotropic velocity renormalization in perfect graphene superlattices, retains a large anisotropic conductivity by inducing strong localization along the hard direction of transport. These results indicate that inevitable sources of disorder can serve as an important tool in tailoring the unique transport properties of graphene.

Acknowledgements— The work by J.G.P. is financially supported by the Danish Council for Independent Research, FTP Grants No. 11-105204 and No. 11-120941. S. R. and A.W.C. acknowledge the Spanish Ministry of Economy and Competitiveness for national project funding (MAT2012-33911) and SAMSUNG for support within the Global Innovation Program. The research leading to these results has received funding from the European Union Seventh Framework Programme under grant agreement n 604391 Graphene Flagship. We thank Antti-Pekka Jauho for helpful comments on the manuscript.

[1] M. I. Katsnelson, K. S. Novoselov, and A. K. Geim, Nat. Phys. **2**, 620 (2006).

[2] E. McCann, K. Kechedzhi, V. I. Falko, H. Suzuura, T. Ando, and B. L. Altshuler, Phys. Rev. Lett. **97**, 146805 (2006); F. V. Tikhonenko, A. A. Kozikov, A. K. Savchenko, and R. V. Gorbachev, Phys. Rev. Lett. **103**, 226801 (2009); P. M. Ostrovsky, I.V. Gornyi, and A. D. Mirlin, Phys. Rev. B **74**, 235443 (2006); K. Nomura and A. H. MacDonald, Phys. Rev. Lett. **98**, 076602 (2007).P. M. Ostrovsky, M. Titov, S. Bera, I.V. Gornyi, and A. D. Mirlin, Phys. Rev. Lett. **105**, 266803 (2010).

[3] P. A. Lee and T. V. Ramakrishnan, Rev. Mod. Phys. **57**, 287 (1985).

[4] F. Evers and A. D. Mirlin, Rev. Mod. Phys. **80**, 1355 (2008).

[5] K. S. Novoselov, V. I. Falko, L. Colombo, P. R. Gellert, M. G. Schwab, and K. Kim, Nature **490**, 192 (2012).

[6] D. A. Areshkin and C. T. White, Nano Lett. **7**, 3253 (2007).

[7] J. T. Kim and S.-Y. Choi, Opt. Express **19**, 24557 (2011).

[8] H. Yan, X. Li, B. Chandra, G. Tulevski, Y. Wu, M. Freitag, W. Zhu, P. Avouris, and F. Xia, Nat. Nanotechnol. **7**, 330 (2012).

[9] M. Yakes, D. Gunlicke, J. L. Tedesco, P. M. Campbell, R. L. Myers-Ward, C. R. Eddy, P. E. Kurt Gaskill, D. Sheehan, and A. R. Laracuente, Nano Lett. **5**, 1559 (2010).

[10] G.-X. Ni, Y. Zheng, S. Bae, H. R. Kim, A. Pachoud, Y. S. Kim, C.-L. Tan, D. Im, J.-H. Ahn, B. H. Hong, et al., ACS Nano **6**, 1158 (2012).

[11] J. P. Robinson, H. Schomerus, L. Oroszlany, and V. I. Falko, Phys. Rev. Lett. **101**, 196803 (2008); A. Lherbier, X. Blase, Y.M. Niquet, F. Triozon, and S. Roche, Phys. Rev. Lett. **101**, 036808 (2008), T. O.Wehling, S. Yuan, A. I. Lichtenstein, A. K. Geim, and M. I. Katsnelson, Phys. Rev. Lett. **105**, 056802 (2010).

[12] C.-H. Park, L. Yang, Y.-W. Son, M. V. Cohen, and S. G. Louie, Nat. Phys. **4**, 213 (2008).

[13] T. G. Pedersen, C. Flindt, J. Pedersen, N. A. Mortensen, A.-P. Jauho, and K. Pedersen, Phys. Rev. Lett **100**, 136804 (2008); J. A. Fürst, J. G. Pedersen, C. Flindt, N. A. Mortensen, M. Brandbyge, T. G. Pedersen, and A.-P. Jauho New. J. Phys. **11**, 095020 (2009).

[14] A. J. M. Giesbers, E. C. Peters, M. Burghard, and K. Kern, Phys. Rev. B **86**, 045445 (2012).

[15] J. Eroms and D. Weiss, New J. Phys. **11**, 095021 (2009).

[16] S. Yuan, R. Roldan, A.-P. Jauho, and M. I. Katsnelson Phys. Rev. B **87**, 085430 (2013).

[17] J. G. Pedersen, T. Gunst, T. Markussen, and T. G. Pedersen, Phys. Rev. B **86**, 245410 (2012); J. G. Pedersen and T. G. Pedersen, Phys. Rev. B **87**, 235404 (2013).

[18] P. D. Garcia, R. Sapienza, C. Toninelli, C. Lopez, and D. S. Wiersma, Phys. Rev. A **84**, 023813 (2011).

[19] T. Gunst, T. Markussen, A.-P. Jauho, and M. Brandbyge, Phys. Rev. B **84** 155449 (2011).

[20] S. Roche and D. Mayou, Phys. Rev. Lett. **79**, 2518 (1997).

[21] A. Lherbier, X. Blase, Y.-M. Niquet, F. Triozon, and S. Roche, Phys. Rev. Lett. **101**, 036808 (2008).

[22] H. Ishii, F. Triozon, N. Kobayashi, K. Hirose, and S. Roche, C. R. Physique **10**, 283 (2009).

[23] L. E. F. Foa Torres, S. Roche, and J. C. Charlier, Introduction to Graphene-Based Nanomaterials: From Electronic Structure to Quantum Transport (Cambridge University Press, Cambridge, 2014).

[24] R. Haydock, Comput. Phys. Commun, **20**, 11 (1980).

[25] J. Bai, X. Zhong, S. Jiang, Y. Huang, X. Duan, Nature Nanotechnology **5**, 190 - 194 (2010); I. Jung, H. Y. Jang and S. Park, Appl. Phys. Lett. **103**, 023105 (2013); J. Liu, H. Cai, X. Yu , K. Zhang, X. Li , J. Li, N. Pan, Q. Shi, Y. Luo, and X. Wang, J. Phys. Chem. C, **116** (29), 15741 (2012).

[26] T. M. Radchenko, A. A. Shylau, and I. V. Zozoulenko, Phys. Rev. B **86**, 035418 (2012).

[27] M. Vanević, V. M. Stojanović, and M. Kindermann, Phys. Rev. B **80**, 045410 (2009).

[28] K. Nomura and A. H. MacDonald, Phys. Rev. Lett. **96**, 256602 (2006).

[29] Y. Y. Zhang, J. Hu, B. A. Bernevig, X. R. Wang, X. C. Xie, and W. M. Liu, Phys. Rev. Le **102**, 106401 (2009).

[30] F. Ortmann, A. Cresti, G. Montambaux, and S. Roche, Europhys. Lett. **94**, 47006 (2011).
[31] A. Lherbier, Simon M.-M. Dubois, X. Declerck, S. Roche, Y.-M. Niquet, and J.-C. Charlier, Phys. Rev. Lett. **106**, 046803 (2011).
[32] S. Roche, N. Leconte, F. Ortmann, A. Lherbier, and D. Soriano, Sol. Stat. Commun. **152**, 1404 (2012).
[33] J. Moser, H. Tao, S. Roche, F. Alsina, C. M. Sotomayor Torres, and A. Bachtold, Phys. Rev. B **81**, 205445 (2010).
[34] A. Barelli, J. Bellissard, and F. Claro Phys. Rev. Lett. **83**, 5082 (1999).